JOURNAL OF GUIDANCE, CONTROL, AND DYNAMICS
Vol. 20, No. 1, January–February 1997

Uncertainty Modeling and Fixed-Order Controller Design for a Hypersonic Vehicle Model

Harald Buschek* and Anthony J. Calise†
Georgia Institute of Technology, Atlanta, Georgia 30332-0150

Control system design for hypersonic vehicles will be complicated by coupling effects between aerodynamics, propulsion, and structure. Using H_∞ and μ-synthesis techniques, these features can be modeled as uncertainties and incorporated into the design procedure of a flight control system. However, modern control theory techniques generally lead to high-order controllers. The time delays, which are created when these controllers are implemented, may not be acceptable. A technique to constrain controller dimension a priori in the design process is used to design fixed-order μ controllers that are robust to mixed real/complex uncertainties. Typical hypersonic effects such as propulsion system perturbations and aeroelastic fuselage bending are modeled as uncertainties in a robust control design framework. Three different fixed-order controllers are synthesized for a hypersonic vehicle model accelerating through Mach 8. A comparison with full-order and reduced-order designs is conducted and the results illustrate that the fixed-order controllers exhibit robustness properties similar to full-order designs while considerably reducing controller complexity.

Introduction

SINGLE-stage-to-orbit vehicles are envisioned to be the launch systems of the next century. Full reusability, horizontal takeoff and landing capability, and short turnaround times are key factors when designing a cost-efficient vehicle for transporting payloads into orbit. However, a variety of technological challenges will have to be overcome that have not been addressed before in the development of one single vehicle. A dominating feature will be a strong interaction between aerodynamics, structure, and propulsion system and the subsequent impact on performance, guidance, and control characteristics.[1] As a result, exceptional requirements will be posed on the flight control system, which not only has to stabilize the vehicle but also has to meet performance specifications such as tracking a desired trajectory while minimizing control effort. Furthermore, wind-tunnel data will be very limited in hypersonic speed regimes above Mach 5. Initial modeling will have to rely heavily on numerical algorithms to predict the aerodynamic and propulsive characteristics of the vehicle. Flight tests of full-scale or reduced-scale test vehicles will be needed to improve and refine the available data. Therefore, the initial flight control system for such a test vehicle will have to be extremely robust towards modeling uncertainties. As more data become available through flight testing, conservatism in the control system can be reduced resulting in increased performance. The flight controllers synthesized in this paper are intended to represent an initial design stage with emphasis on robustness to typical hypersonic effects that are not encountered with any other class of air- or spacecraft.

In hypersonic propulsion, the entire vehicle aerodynamic configuration must be considered as part of the propulsion system. Before reaching the inlet, the external flow will be compressed along the forebody, and after leaving the combustor the aftbody is utilized as an external nozzle. Changing the angle of attack for control purposes alters these flowfields and results in variations in thrust vector magnitude and direction influencing stability and control of the vehicle. The need for a low structural weight mass fraction introduces relatively low structural vibration frequencies. Significant elastic/rigid body mode interactions are likely to occur, imposing additional requirements on the flight control system. Additionally, bending of the forebody influences the flow conditions at the inlet, which propagates through the engine and together with the elastic deformation of the aftbody again affects the thrust vector. Determination of the elastic mode shapes will initially be highly uncertain.

These effects are modeled as uncertainties in the context of a robust control study. It has been shown in Refs. 2 and 3 that modern control theory using H_∞ and μ-synthesis techniques is well suited for addressing multiple uncertainty sources in hypersonic flight control design. However, a significant disadvantage of these techniques is that the resulting controller is of the same order as the generalized plant. Frequency dependent weights have to be included in the design framework to achieve the desired performance and robustness characteristics. Thus, the order of the generalized plant is increased resulting in high-order controllers. When implemented, large-order controllers can create time delays, which may be undesirable. One solution to this problem is to use model order reduction on the controller realization. This technique, though, does not consider the properties of the closed-loop system when reducing the order of the controller and, therefore, robustness properties are not guaranteed. Another approach to this problem is to constrain the order of the controller a priori in the design process.

If multiple uncertainty sources are present in the system, H_∞ controllers will be too conservative because they do not account for the structure in the uncertainty. The μ-synthesis technique alleviates this problem but is still conservative in that only complex representations of uncertainty models are considered. For real parameter uncertainty, this representation can be conservative. The capacity to model variations in real parameters is currently an active research area.

A flight control system for a hypersonic vehicle with airbreathing propulsion accelerating through Mach 8 is designed. A novel approach to synthesize controllers of constrained dimensions with robustness to mixed real/complex uncertainties is used. The vehicle configuration and the development of uncertainty models for propulsion system perturbations, aeroelastic fuselage effects, and variations in control effectiveness are described. In the framework of a robust control study, a full-order and three different fixed-order mixed μ controllers are synthesized and their performance is evaluated in a linear simulation using a worst-case disturbance.

Fixed-Order Controllers with Robustness to Mixed Real/Complex Uncertainties

A thorough description of the fixed-order mixed μ controller design procedure and its theoretical background is provided in Ref. 4.

Presented as Paper 95-6062 at the AIAA/AAAF/DGLR/JSASS/RAeS 6th International Aerospace Plane and Hypersonics Technologies Conference, Chattanooga, TN, April 3–7, 1995; received April 28, 1995; revision received June 10, 1996; accepted for publication Aug. 30, 1996.

*Graduate Research Assistant, School of Aerospace Engineering; currently Research Engineer, Bodenseewerk Gerätetechnik GmbH (BGT), P.O. Box 101155, D-88641 Überlingen, Germany. Member AIAA.

†Professor, School of Aerospace Engineering. Fellow AIAA.

Therefore, only a concise introduction into the principles of the fixed-order design technique and the mixed μ-synthesis procedure is provided.

Fixed-order design is performed by enforcing a constraint on the controller order a priori in the design process. The current technique utilizes a controller canonical form, which is imposed on the compensator structure,

$$\dot{\boldsymbol{x}}_c = P^0 \boldsymbol{x}_c + N^0 \boldsymbol{u}_c - N^0 \boldsymbol{y} \tag{1}$$

$$\boldsymbol{u}_c = -P \boldsymbol{x}_c \tag{2}$$

$$\boldsymbol{u} = -H \boldsymbol{x}_c \tag{3}$$

where $\boldsymbol{x}_c \in \mathcal{R}^{nc}$ is the controller state vector of fixed dimension nc, $\boldsymbol{u}_c \in \mathcal{R}^{ny}$ is an internal feedback vector, $\boldsymbol{y} \in \mathcal{R}^{ny}$ is the measurement vector, and $\boldsymbol{u} \in \mathcal{R}^{nu}$ is the control vector. P^0 and N^0 are fixed matrices of zeros and ones, and P and H are free-parameter matrices.[5] With this formulation, the compensator states can be absorbed in the generalized plant to define a static gain output feedback problem. The free parameters of P and H are embedded in the static gain feedback matrix G.

A differential game formulation for the H_∞ optimization problem of the closed-loop system from disturbance inputs $\boldsymbol{w}$ to performance outputs $\boldsymbol{z}$, T_{zw}, is employed, and a worst-case disturbance model is introduced.[6] This allows the derivation of three first-order necessary conditions for an H_∞-optimal fixed-order controller,

$$\left(\tilde{A} + \gamma^{-2} \tilde{B} \tilde{B}^T Q_\infty\right) L + L \left(\tilde{A} + \gamma^{-2} \tilde{B} \tilde{B}^T Q_\infty\right)^T + \tilde{B} \tilde{B}^T = 0 \tag{4}$$

$$\tilde{A}^T Q_\infty + Q_\infty \tilde{A} + \tilde{C}^T \tilde{C} + \gamma^{-2} Q_\infty \tilde{B} \tilde{B}^T Q_\infty = 0 \tag{5}$$

$$2\left(\bar{D}_{12}^T \bar{D}_{12} G \bar{C}_2 - \bar{D}_{12}^T \bar{C}_1 - \bar{B}_2 Q_\infty\right) L \bar{C}_2^T = 0 \tag{6}$$

$\tilde{A}$, $\tilde{B}$, and $\tilde{C}$ are the system matrices of the closed-loop system T_{zw} and are dependent on the free-parameter gain matrix G. $\bar{B}$, $\bar{C}$, and $\bar{D}$ and their respective partitions refer to the augmented open-loop system in the static gain output feedback problem. The upper bound on the ∞-norm of the closed-loop system is denoted by γ. These necessary conditions are coupled in L, Q_∞, and G and are solved using a homotopy algorithm.[7] The homotopy algorithm requires a low-order, stabilizing initial guess, which is gradually deformed until the suboptimal fixed-order H_∞ controller is obtained. One possible approach to derive an initial guess is to employ order reduction on a full-order H_∞ or H_2 controller designed for the given problem.[4] The only requirement is that the initial guess stabilizes the closed-loop system.

To reduce conservatism in the design procedure, a mixed real/complex μ-synthesis method is employed. As in complex μ-synthesis, this technique accounts for the structure in the uncertainty. Furthermore, real parameter uncertainty is considered reducing conservatism even more. The issue of real parameter uncertainty has received considerable attention over the past years and various approaches have been developed (see, for example, Refs. 8 and 9). The method employed in the current controller design procedure is the so-called D,G–K iteration introduced in Ref. 10. In addition to the D-scales matrices of complex μ-synthesis, the so-called G-scales matrices are defined to capture the phase properties of real parameters. This allows a refinement of the upper bound on the structured singular value μ, which is a measure of achievable robust performance in the face of structured uncertainty. The result is an iterative procedure where alternately full-order H_∞ controllers and optimal scaling matrices are designed until achievable robust performance cannot be improved anymore.

The fact that H_∞ design is a subproblem in the mixed μ-synthesis procedure using D,G–K iteration allows replacing the full-order controller design step with the fixed-order technique described earlier. This leads to a fixed-order mixed μ-synthesis technique capable of designing low-order μ controllers with significantly reduced conservatism.

Hypersonic Vehicle Model

The hypersonic vehicle model used in this study is the winged-cone configuration described in Ref. 11. Main characteristics of this vehicle are an axisymmetric conical forebody, a cylindrical engine nacelle section with engine modules all around the body, and a cone frustrum engine nozzle section (see Fig. 1). To carry out control studies, a five-state linear model of the longitudinal dynamics is used representing flight conditions for an accelerated flight through Mach 8 at approximately 86,000 ft. State and control variables are

$$\boldsymbol{x} = \begin{bmatrix} V \\ \alpha \\ q \\ \theta \\ h \end{bmatrix} = \begin{bmatrix} \text{velocity (ft/s)} \\ \text{angle of attack (deg)} \\ \text{pitch rate (deg/s)} \\ \text{pitch attitude (deg)} \\ \text{altitude (ft)} \end{bmatrix} \tag{7}$$

$$\boldsymbol{u} = \begin{bmatrix} \delta e \\ \delta \eta \end{bmatrix} = \begin{bmatrix} \text{symmetric elevon (deg)} \\ \text{fuel equivalence ratio} \end{bmatrix} \tag{8}$$

The fuel equivalence ratio is defined as

$$\eta = \frac{\dot{m}_f / \dot{m}_{\text{air}}}{(\dot{m}_f / \dot{m}_{\text{air}})_{\text{stoichiometric}}} \tag{9}$$

where $\dot{m}_f$ and $\dot{m}_{\text{air}}$ are fuel and air mass flow rates, respectively. The system matrices are given by

$$A = \begin{bmatrix} 3.6524e{-}3 & -9.6679e{-}1 & 0.0000 & -5.5639e{-}1 & -1.4321e{-}3 \\ -3.9195e{-}5 & -8.1626e{-}2 & 1.0000 & -8.4420e{-}5 & 9.2560e{-}6 \\ 2.0147e{-}3 & 3.0354 & -9.5218e{-}2 & 1.5500e{-}5 & -1.0766e{-}5 \\ 2.7263e{-}6 & 7.7679e{-}6 & 1.0000 & -7.7679e{-}6 & -1.0188e{-}9 \\ 2.0779e{-}2 & -1.3701e{-}2 & 0.0000 & 1.3701e{-}2 & 0.0000 \end{bmatrix} \tag{10}$$

$$B = \begin{bmatrix} 9.6995e{-}2 & 7.5989 \\ 3.3486e{-}3 & -2.0942e{-}3 \\ 1.0825 & 0.0000 \\ 0.0000 & 0.0000 \\ 0.0000 & 0.0000 \end{bmatrix} \tag{11}$$

Because the linear model is defined for a trimmed, accelerated flight condition, the state and control variables are perturbation quantities representing deviations from a climbing and accelerating flight condition. This model represents pure rigid-body dynamics and, therefore, does not account for any aeroelastic effects. Also,

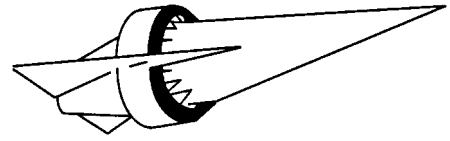

Fig. 1 Hypersonic winged-cone accelerator.

the propulsion system model used for the winged-cone configuration does not include sensitivity to angle-of-attack variations.

The interconnection structure for controller design is shown in Fig. 2 and is derived from the study in Ref. 2. The design is carried out as a velocity and altitude command tracking system. Velocity error, altitude error, pitch rate, and pitch attitude are the measurements fed back to the controller. Control actuator dynamics are represented by first-order filters with 30-rad/s bandwidth for elevon and 100-rad/s bandwidth for fuel equivalence ratio.

Dryden turbulence models are used to introduce atmospheric disturbances. The turbulence spectrum is defined by the weights

$$F_u(s) = \sqrt{\frac{2V_0\sigma_u^2}{L_u}}\,\frac{1}{s + V_0/L_u} \tag{12}$$

for longitudinal and

$$F_w(s) = \sqrt{\frac{3V_0\sigma_w^2}{L_w}}\,\frac{s + V_0/(\sqrt{3}L_w)}{(s + V_0/L_w)^2} \tag{13}$$

for vertical wind gusts.[12] For the reference altitude used in this study[13]

$$\sigma_u = 10.8 \text{ ft/s}, \qquad \sigma_w = 6.88 \text{ ft/s} \tag{14}$$

$$L_u = 65{,}574 \text{ ft}, \qquad L_w = 26{,}229 \text{ ft} \tag{15}$$

Weights are imposed on control deflections and actuator rates to minimize control effort and to reduce the sensitivity of the control response to atmospheric disturbances. These weights are considered design parameters in the H_∞-synthesis procedure. They have to be adjusted in the design process until the control responses of the resulting H_∞ controller are satisfactory. Several full-order design iterations resulted in the following weights:

$$W_{\delta e} = 3, \qquad W_{\delta\eta} = 3 \tag{16}$$

$$W_{\dot{\delta} e} = 5, \qquad W_{\dot{\delta}\eta} = 1 \tag{17}$$

To guarantee natural responses in velocity and altitude, command tracking is pursued using a model following approach. The velocity command is passed through a first-order filter, where the time constant is selected to result in a 5% settling time of approximately 60 s,

$$W_{Vc} = \frac{0.05}{s + 0.05} \tag{18}$$

Since the velocity signal has to be integrated one more time to obtain altitude, the altitude command is shaped by a second-order transfer function

$$W_{hc} = \frac{\omega_n^2}{s^2 + 2\zeta\omega_n s + \omega_n^2} \tag{19}$$

where a damping ratio of $\zeta = 0.8$ and a desired settling time of 80 s result in a natural frequency of $\omega_n = 0.0468$ rad/s. With this approach constant weights on the error signals velocity and altitude suffice to ensure a small steady-state error and a transient response consistent with the vehicle's natural dynamics. The weights were adjusted together with weights on the control, which resulted in the following values:

$$W_V = 3, \qquad W_h = 1 \tag{20}$$

The model following approach proved to be a critical step toward defining a round system that avoids numerical difficulties in the controller synthesis. A measurement noise weight

$$W_{\text{noise}} = 10^{-4} I_4 \tag{21}$$

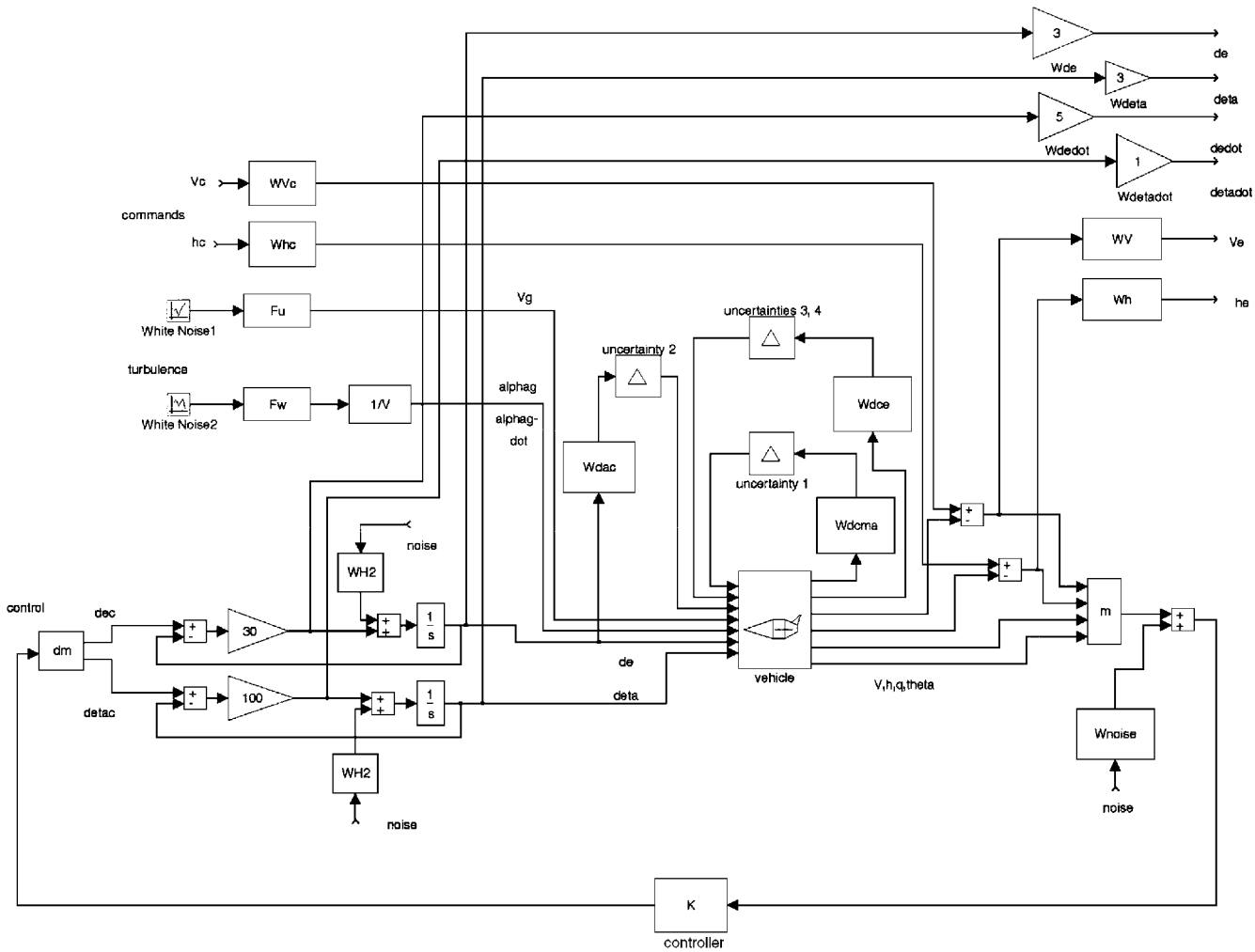

Fig. 2 Interconnection structure for controller design.

is employed for all of the fedback variables. The noise model is not intended to represent realistic sensor data but has to be included because the application of H_∞ theory to output feedback problems requires that all measurement signals be corrupted by noise.

The actuator modes are not controllable from the disturbance input. This is normally not a problem since these modes are stable. However, as described in Ref. 4, one possibility to obtain an initially stabilizing fixed-order controller is a low-authority H_2 design, which is followed by an order reduction, followed by transformation to controller canonical form. This last step requires that the input matrix for the reduced-order compensator (which is the optimal filter gain in the full-order case) be full rank. This is not the case if the plant is not controllable from the disturbance input. Therefore, two independent white noise processes are injected into the actuators with intensity

$$W_{H2} = 10^{-4} \tag{22}$$

to satisfy this condition.

Uncertainty Modeling

Aerospace vehicles in hypersonic flight regimes will typically utilize scramjet propulsion systems, which are highly integrated into the airframe. This results in an increased sensitivity to variations in angle of attack.[14] The most important impact of these propulsive perturbations is on the pitching moment leading to significant control surface deflections to stabilize the vehicle.[15] This phenomenon is addressed as parametric uncertainty in the pitching moment sensitivity to angle-of-attack variations $c_{M\alpha}$. The uncertainty is represented by a scalar perturbation to the nominal model. This perturbation can be rearranged to obtain input and output quantities d_Δ and e_Δ. The matrices B_Δ, C_Δ, and D_Δ can be chosen from the uncertain model

$$\begin{aligned} \dot{\boldsymbol{x}} &= A\boldsymbol{x} + B\boldsymbol{u} + B_\Delta \boldsymbol{d}_{\boldsymbol{\Delta}} & \boldsymbol{e}_{\boldsymbol{\Delta}} &= C_\Delta \boldsymbol{x} + D_\Delta \boldsymbol{u} \\ \boldsymbol{y} &= C\boldsymbol{x} + D\boldsymbol{u} & \boldsymbol{d}_{\boldsymbol{\Delta}} &= \Delta \boldsymbol{e}_{\boldsymbol{\Delta}} \end{aligned} \tag{23}$$

If a scaling has been applied so that the values of Δ range between -1 and 1, Eq. (23) represents the set of all possible models. Δ in this case is a scalar because only one parameter is perturbed. For the case of uncertainty in the parameter $c_{M\alpha}$, which occurs in the (3,2) element of the A matrix, the uncertainty matrices are

$$B_\Delta = [0 \quad 0 \quad 1 \quad 0 \quad 0]^T \tag{24}$$

$$C_\Delta = [0 \quad 1 \quad 0 \quad 0 \quad 0] \tag{25}$$

$$D_\Delta = 0 \tag{26}$$

This uncertainty is labeled uncertainty 1 in Fig. 2.

Significant coupling between the elastic- and rigid-body modes is expected for this vehicle type, which has to be considered in the design of a robust flight control system. Moreover, fuselage bending affects propulsion system performance via perturbed inflow conditions, which in turn influences the rigid-body flight dynamics or even excites the elastic modes.[16] Because the model used in this study comprises only rigid-body dynamics and no aeroelastic information on the winged-cone accelerator was available, a simple yet concise method had to be developed to introduce aeroelastic effects as uncertainty into the rigid-body behavior.

Based on elementary theory in structural dynamics,[17] a second-order transfer function was derived exhibiting elastic deformations of a long, slender, uniform body caused by a force $P(s)$ suddenly applied at a certain location of the body x_p,

$$\theta_i(x, s) = \frac{\phi_i(x_p)[\mathrm{d}\phi_i(x)/\mathrm{d}x]}{\left(s^2 + 2\zeta_i\omega_i s + \omega_i^2\right) M_i} P(s) \tag{27}$$

where $\theta_i(x, s)$ is the angle by which the deformed body is deflected from its original shape due to the ith elastic mode; $\phi_i(x)$ is the mode shape function of the ith elastic mode; ζ_i and ω_i are the corresponding damping ratio and natural frequency, respectively; and M_i is the modal mass defined by

$$M_i = \int_0^L m(x)\phi_i^2(x)\,\mathrm{d}x \tag{28}$$

where $m(x)$ is the mass distribution and L the length of the body. In the case of the winged cone vehicle, structural excitement is caused by lift increments due to elevon deflections

$$\begin{aligned} P(s) &= \delta L(s) \\ &= 2\frac{\partial c_{L,da}}{\partial \delta e}\, q\, S_{\mathrm{ref}}\, \delta e(s) \end{aligned} \tag{29}$$

where q is the dynamic pressure for the given flight condition, S_{ref} the reference area, and $\partial c_{L,da}/\partial \delta e$ the sensitivity of the lift coefficient of one elevon to the elevon deflection. This was graphically determined from Ref. 11. The body deflection angle $\theta(x, s)$ can also be interpreted as change in the angle of attack $\Delta\alpha(x, s)$ due to elastic deformation. As previously mentioned, angle-of-attack perturbations affect the rigid-body dynamics via the propulsion system; thus, the transfer function given in Eq. (27) is evaluated at the location of the inlet entrance. The resulting estimation of the angle-of-attack variation due to flexible body motion excited by elevon deflections is then fed as uncertainty into the rigid-body model, using the second column of the nominal plant A matrix [see Fig. 2 and Eqs. (7) and (10)].

Unfortunately, no information on the mode shapes $\phi_i(x)$ of the winged-cone accelerator was available for this study. Thus, the rather crude assumption of a uniform beam with both ends free was chosen to model the elastic mode shapes. The analytical solution to this problem can be found in any textbook on structural dynamics (e.g., Ref. 17). The natural frequencies are taken from a generic National Aero-Space Plane configuration investigated in Ref. 18. The first three fuselage bending modes of the unheated vehicle are considered and are given by $\omega_1 = 2.95$ Hz, $\omega_2 = 5.72$ Hz, and $\omega_3 = 7.74$ Hz. The damping ratio for structural vibration modes is typically small and was chosen to be $\zeta_i = 0.01$ for all three frequencies. The frequency response of the resulting flexible mode function in Eq. (27) is shown in Fig. 3. Because of the uniform beam approximation an amplification was necessary to achieve a reasonable response magnitude. Also given in Fig. 3 is the response of the rigid body due to elevon deflections and a cover function that was used for the controller design. The cover function is given by

$$W_{dac} = \frac{k_c(s+2)}{s^2 + 2\zeta_c\omega_c s + \omega_c^2} \tag{30}$$

with $k_c = 2.5$, $\zeta_c = 0.25$, and $\omega_c = 19.53$ rad/s.

The effect of aerodynamic heating during high-speed flight through the atmosphere on the elastic characteristics of a hypersonic vehicle was addressed in Ref. 18. One conclusion was that for increasing aerothermal heating loads (related to increasing Mach numbers) the natural frequencies of the fuselage bending modes decreased. This invokes the potential of rigid/elastic body mode coupling. The frequency response when the natural frequencies are reduced to 60% of their values for the unheated vehicle is also

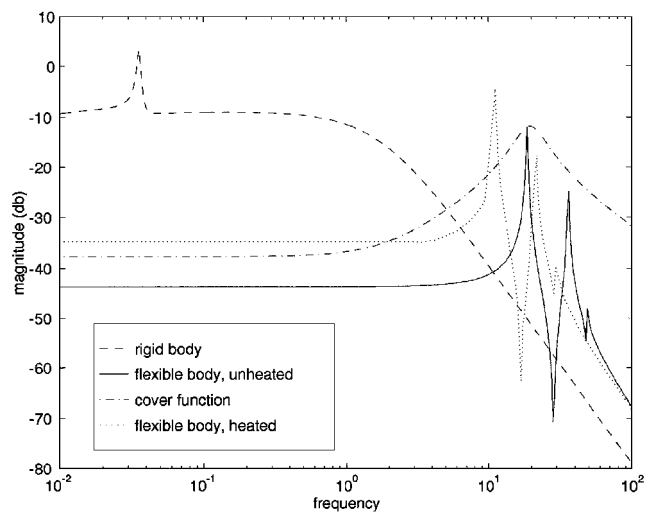

Fig. 3 Angle-of-attack responses to elevon input.

given in Fig. 3. As the elastic-mode frequencies approach the rigid-body frequencies, the level of uncertainty introduced into the system increases. Accordingly, the parameters of the cover function for controller design need to be adjusted to account for the changed flexible-body behavior (not shown in Fig. 3). The effect of aerodynamic heating on control system design and achievable robust performance is investigated in Ref. 3. The uncertainty model for aeroelastic deformation is labeled uncertainty 2 in Fig. 2.

In addition to uncertainty models representing typical hypersonic effects for an integrated flight control design, uncertainty in control effectiveness is also accounted for. Both elevon and fuel equivalence ratio control channels are considered. Variations in control effectiveness are modeled as parametric uncertainties in pitching moment sensitivity to elevon deflections $c_{M\delta e}$ and in thrust sensitivity to fuel flow variations $c_{T\delta\eta}$. These parameters are the (3, 1) element and the (1, 2) element in the B matrix, respectively, and are modeled according to the framework in Eq. (23). These uncertainties are labeled uncertainties 3, 4 in Fig. 2.

Robust Performance Study

To conduct a robust performance study, the uncertainty models representing typical hypersonic effects are implemented in the general controller design framework. For propulsion system perturbations, 25% uncertainty in $c_{M\alpha}$ was introduced:

$$W_{dcma} = 0.25 \cdot A(3, 2) \tag{31}$$

The cover function W_{dac} in Eq. (30) was used to represent the effects of aeroelastic deformations on the unheated vehicle. Uncertainty levels in control effectiveness were chosen to be 10% resulting in the weight

$$W_{dce} = \begin{bmatrix} 0.1 \cdot B(3, 1) & 0 \\ 0 & 0.1 \cdot B(1, 2) \end{bmatrix} \tag{32}$$

Since no information on the magnitude of the described perturbations was available, the uncertainty levels in W_{dcma} and W_{dce} were chosen rather small to ascertain whether robust performance is achievable for the given problem. Hence, three real parameter uncertainties (W_{dcma}, W_{dce}) and one complex uncertainty (W_{dac}) are incorporated into the system. The inclusion of the uncertainty models leads to a robust performance problem with structured uncertainty. The inherent conservatism when this structure is not accounted for is demonstrated by a full-order H_∞ design: the peak value of the upper bound on robust performance is in this case $\mu = 51.47$.

In a first design step, full-order μ controllers using both complex and mixed μ-synthesis were designed. The complex μ controller was 35th order and achieved a peak value of 1.281 for the complex upper μ bound. The mixed μ controller had 12 additional states due to the G-scales resulting in a 47th-order compensator. The improvement over the complex controller, however, was only marginal, and a peak value of 1.223 of the mixed upper μ bound was achieved. In contrast to the results in Ref. 4, both complex and mixed μ controllers achieve similar robust performance levels in this case. The rather aggressive approach of allowing only 25 and 10% uncertainty in the real parameters may contribute to this fact.

Order reduction of the full-order controllers was performed utilizing a variety of reduction schemes: truncation of a balanced realization of the controller, truncation or residualization of the controller transformed in bidiagonal form, optimal Hankel norm approximations using balanced and unbalanced realizations, and a Schur method model reduction. These methods are available in commercial software packages.[19,20] However, order reduction of the controller does not guarantee robust stability or robust performance of the closed-loop system. It has been observed in this study that controllers reduced with the balanced truncation scheme tended to yield best results with respect to achieving closed-loop stability and performance. Therefore, this method is used to reduce the mixed μ controller to ninth and fifth order. Their peak values were $\mu = 1.964$ and 9.228, respectively. In particular, the fifth-order reduced controller exhibits a significant loss of robust performance. Reduced seventh-order controllers were obtained using all of the reduction methods mentioned. However, none of them stabilized the closed-loop system.

Table 1 Values of μ for full-, reduced-, and fixed-order controllers

	Complex μ full (number of states)	Mixed μ full (number of states)	Mixed μ reduced	Mixed μ fixed
Full order	1.281 (35)	1.223 (47)	——	——
Ninth order	——	——	1.964	1.245
Seventh order	——	——	Unstable	1.264
Fifth order	——	——	9.228	1.330

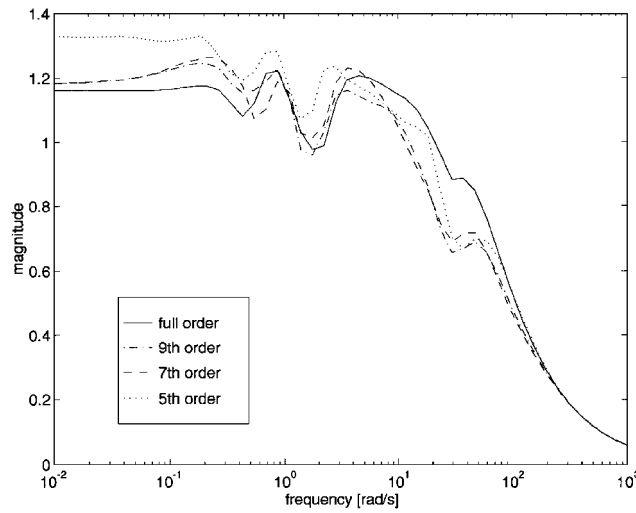

Fig. 4 Robust performance bounds of full- and fixed-order μ controllers.

According to the fixed-order design procedures outlined in the second section, the reduced ninth- and fifth-order controllers were used as starting guesses for the fixed-order algorithm. In the case of the ninth-order compensator, one single fixed-order design step sufficed to decrease the upper mixed μ bound to 1.245. The full-order robust performance level could almost be recovered. The fifth-order controller required one additional D,G–K iteration and achieved $\mu = 1.330$. The results are summarized in Table 1.

As already mentioned, a seventh-order reduced controller could not be obtained directly. However, order reduction of the previously synthesized fixed ninth-order design resulted in a seventh-order controller, which was internally stabilizing. This controller was used as a starting guess, and after one additional fixed-order D,G–K iteration, the resulting fixed seventh-order design achieved an upper mixed μ bound of $\mu = 1.264$. This result complements the ninth- and fifth-order designs in Table 1 and demonstrates the consistency in achievable robust performance for the three different fixed-order controllers. The upper mixed μ bounds of the closed-loop systems with the full-order and the three fixed-order mixed μ controllers implemented are shown in Fig. 4.

Implementing the different mixed μ controllers, time simulations were conducted for simultaneous step commands in velocity and altitude of $V_c = 100$ ft/s and $h_c = 1000$ ft while encountering longitudinal and vertical atmospheric turbulence. The time simulations were carried out using the linear model at Mach 8, which suffices at the initial stage of the present design. However, the closed-loop system was perturbed by a worst-case, real-rational, stable perturbation $\Delta_p(s)$ reflecting the effects of worst-case uncertainty and disturbances within the given bounds. This perturbation was obtained by searching for the peak value of the lower μ bound over frequency and constructing the corresponding perturbation such that $I - M\Delta_p = 0$ at this frequency.[20] $\Delta_p(s)$ has the same block structure as the uncertainty. For the full-order mixed μ controller, $\Delta_p(s)$ is given by

$$A_{\text{pert}} = [-0.3219] \tag{33}$$

$$B_{\text{pert}} = [0 \quad -0.7269 \quad 0 \quad 0] \tag{34}$$

$$C_{\text{pert}} = \begin{bmatrix} 0 \\ -0.7269 \\ 0 \\ 0 \end{bmatrix} \tag{35}$$

$$D_{\text{pert}} = \begin{bmatrix} -0.8207 & 0 & 0 & 0 \\ 0 & -0.8207 & 0 & 0 \\ 0 & 0 & 0.8207 & 0 \\ 0 & 0 & 0 & 0.8207 \end{bmatrix} \tag{36}$$

This worst-case perturbation is implemented in place of the Δ in Fig. 2 to carry out the simulations. The same perturbation is also used for the fixed-order controllers to provide a consistent simulation environment. As a consequence of the worst-case disturbance model, the effect of the flexible body dynamics in the time simulations is introduced utilizing the cover function defined in the preceding section.

Velocity and altitude responses of the full- and the fixed-order mixed μ designs are depicted in Figs. 5 and 6. All low-order controllers provide a smooth increase in velocity comparable to the full-order design. The altitude responses in Fig. 6 are also very similar for all designs. The systems using the full-order and the fixed fifth-order controllers exhibit a distinct nonminimum phase behavior. This is not too surprising since the vehicle has to pitch up to increase altitude. The required elevon deflections reduce the overall lift during the initial phase of the maneuver, which can result in a minor loss of altitude.

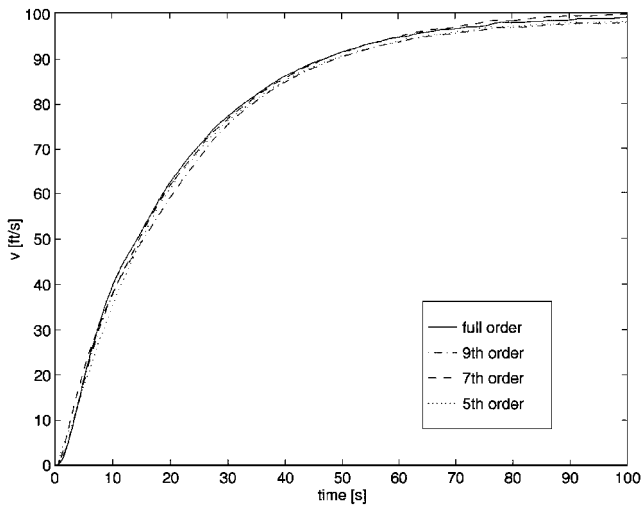

Fig. 5 Velocity responses of mixed μ designs.

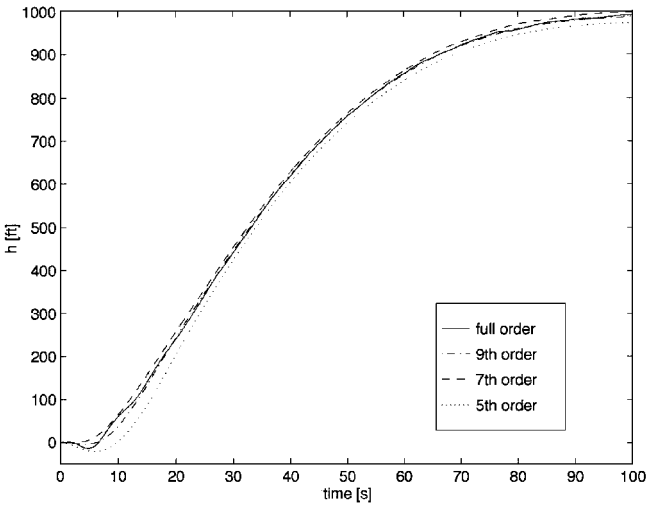

Fig. 6 Altitude responses of mixed μ designs.

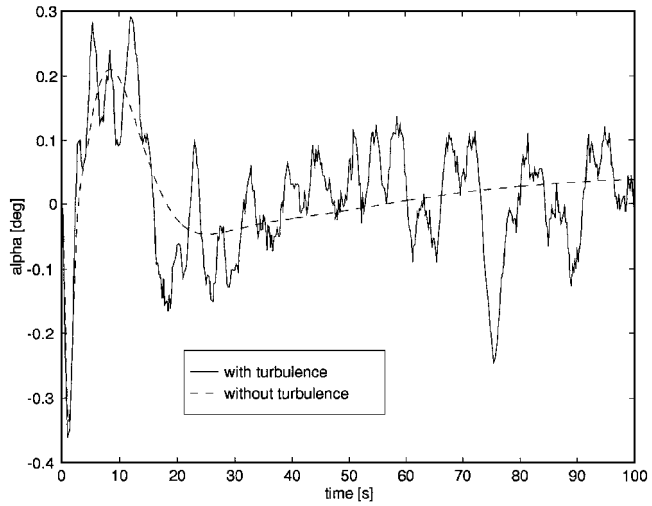

Fig. 7 Angle-of-attack response, fixed fifth-order controller.

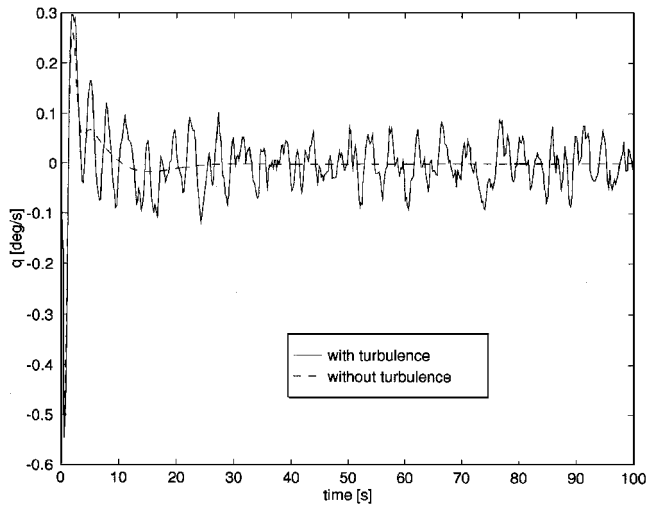

Fig. 8 Pitch rate response, fixed fifth-order controller.

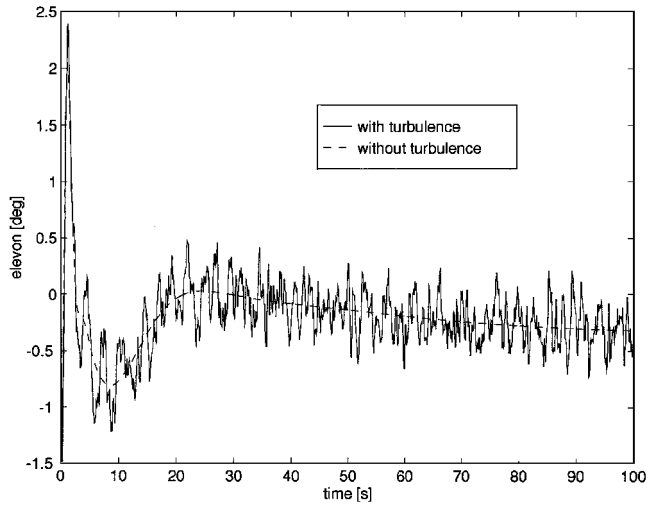

Fig. 9 Elevon control history, fixed fifth-order controller.

Angle-of-attack and pitch rate responses are illustrated for the example of the fixed fifth-order controller in Figs. 7 and 8. After larger variations at the beginning of the maneuver to initiate the climb, considerable oscillations due to atmospheric turbulence dominate the responses. The control histories in elevon and fuel equivalence ratio in Figs. 9 and 10 display the same characteristics, even though the control rates were penalized to reduce sensitivity to turbulence. Noticeable is the relatively large initial elevon deflection, which results in a decrease in the overall lift and leads to the nonminimum phase behavior in the altitude response (Fig. 6).

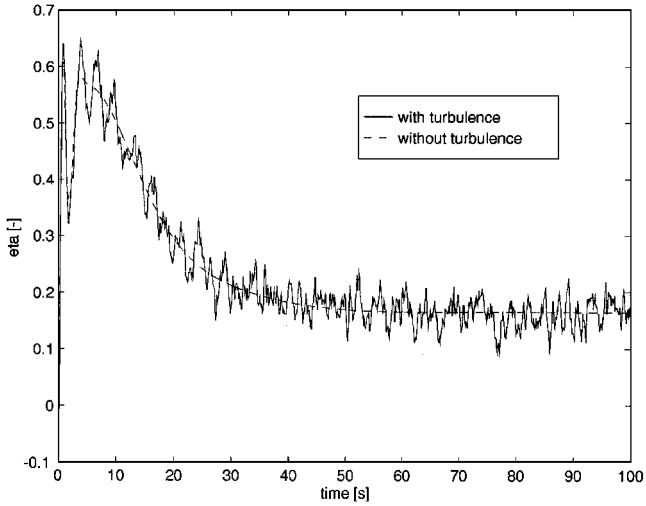

Fig. 10 Equivalence ratio control history, fixed fifth-order controller.

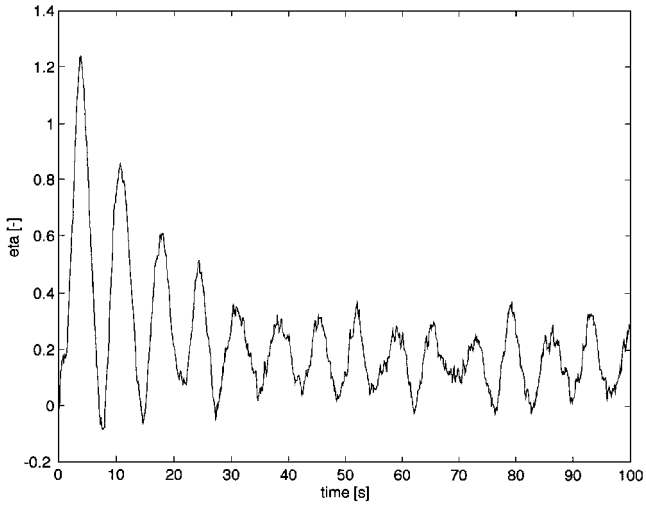

Fig. 11 Equivalence ratio control history, reduced fifth-order controller.

A comparison to reduced-order controllers is conducted by investigating the equivalence ratio response of the reduced fifth-order controller in Fig. 11. Significant oscillations in the control history confirm the loss in robust performance indicated by the large μ value in Table 1.

The results illustrate that all fixed-order controllers meet the performance requirements for tracking commanded velocity and altitude. Moreover, the controllers demonstrate robustness to the impact of atmospheric turbulence and a worst-case disturbance model. However, due to the linear nature of the controller synthesis procedure, these results are only valid in the vicinity of the given flight condition at Mach 8. For different flight conditions, gain scheduled controllers need to be designed.

Conclusions

Uncertainty models for the typical hypersonic effects of propulsion system perturbations, aeroelastic fuselage bending, and variations in control effectiveness have been developed. Robust control designs have been conducted for a hypersonic vehicle model with airbreathing propulsion. Model reduction schemes employed to reduce the dimension of full-order controllers do not guarantee stability or robustness of the closed-loop system. A new technique to synthesize fixed-order controllers with robustness to mixed real/complex uncertainties has been used. It appears in this study that the developed fixed-order design technique can significantly improve both nominal and robust performance. Fixed ninth-, seventh-, and fifth-order controllers achieve robust performance levels comparable to a full-order design with 47 states. Time simulations for simultaneous commands in velocity and altitude while encountering atmospheric turbulence and a worst-case disturbance from the uncertainties confirmed the achievable robust performance of the controllers. The results indicate that the new methodology is feasible for designing control systems for typical future aerospace vehicles.

Acknowledgments

This research has been supported by NASA Langley Research Center under Grant NAG-1-1451 and by the Army Research Office under Grant DAAH 04-93-6-002. A preliminary version of MATLAB^{TM} software to perform the D,G–K iteration procedure was made available by P. M. Young, Laboratory for Information and Decision Systems, Massachusetts Institute of Technology.

References

[1]Schmidt, D. K., Mamich, H., and Chavez, F., "Dynamics and Control of Hypersonic Vehicles—The Integration Challenge for the 1990's," AIAA Paper 91-5057, Dec. 1991.

[2]Gregory, I. M., McMinn, J. D., Shaughnessy, J. D., and Chowdhry, R. S., "Hypersonic Vehicle Control Law Development Using H_∞ and μ-Synthesis," AIAA Paper 92-5010, Dec. 1992.

[3]Buschek, H., and Calise, A. J., "Robust Control of Hypersonic Vehicles Considering Propulsive and Aeroelastic Effects," *Proceedings of the AIAA Guidance, Navigation, and Control Conference* (Monterey, CA), 1993, AIAA, Washington, DC, pp. 550–560 (AIAA Paper 93-3762).

[4]Buschek, H., and Calise, A. J., "μ Controllers: Mixed and Fixed," *Journal of Guidance, Control, and Dynamics*, Vol. 20, No. 1, 1997, pp. 34–41.

[5]Luenberger, D. G., "Canonical Forms for Linear Multivariable Systems," *IEEE Transactions on Automatic Control*, Vol. AC-12, No. 6, 1967, pp. 290–293.

[6]Sweriduk, G. D., and Calise, A. J., "A Differential Game Approach to the Mixed H_2/H_∞ Design Problem," *Proceedings of the AIAA Guidance, Navigation, and Control Conference* (Scottsdale, AZ), 1994, AIAA, Washington, DC, pp. 1072–1082 (AIAA Paper 94-3660).

[7]Whorton, M., Buschek, H., and Calise, A. J., "Homotopy Algorithm for Fixed Order H_2 and H_∞ Design," *Proceedings of the AIAA Guidance, Navigation, and Control Conference* (Scottsdale, AZ), 1994, AIAA, Washington, DC, pp. 1083–1093 (AIAA Paper 94-3661).

[8]Safonov, M. G., Ly, J. H., and Chiang, R. Y., "μ-Synthesis Robust Control: What's Wrong and How to Fix It?," *Proceedings of the 1993 IEEE, Conference on Aerospace Control Systems* (West Lake Village, CA), Inst. of Electrical and Electronics Engineers, Piscataway, NJ, 1993, pp. 563–568.

[9]How, J. P., Haddad, W. M., and Hall, S. R., "Application of Popov Controller Synthesis to Benchmark Problems with Real Parameter Uncertainty," *Journal of Guidance, Control, and Dynamics*, Vol. 17, No. 4, 1994, pp. 759–768.

[10]Young, P. M., "Controller Design with Mixed Uncertainties," *Proceedings of the 1994 American Control Conference* (Baltimore, MD), Inst. of Electrical and Electronics Engineers, Piscataway, NJ, 1994, pp. 2333–2337.

[11]Shaughnessy, J. D., Pinckney, S. Z., McMinn, J. D., Cruz, C. I., and Kelley, M.-L., "Hypersonic Vehicle Simulation Model: Winged-Cone Configuration," NASA TM 102610, Nov. 1990.

[12]Turner, R. E., and Hill, C. K., "Terrestrial Environment (Climatic) Criteria Guidelines for Use in Aerospace Vehicle Development, 1982 Revision," NASA TM 82473, June 1982.

[13]Justus, C. G., Campbell, C. W., Doubleday, M. K., and Johnson, D. L., "New Atmospheric Turbulence Model for Shuttle Applications," NASA TM 4168, Jan. 1990.

[14]Walton, J., "Performance Sensitivity of Hypersonic Vehicles to Changes in Angle of Attack and Dynamic Pressure," AIAA Paper 89-2463, July 1989.

[15]Calise, A. J., and Buschek, H., "Research in Robust Control for Hypersonic Vehicles," Progress Rept. 1 to NASA Langley Research Center, Contract NAG-1-1451, Nov. 1992.

[16]Raney, D. L., McMinn, J. D., Pototzky, A. S., and Wooley, C. L., "Impact of Aeroelasticity on Propulsion and Longitudinal Flight Dynamics of an Air-Breathing Hypersonic Vehicle," *Proceedings of the 34th Structures, Structural Dynamics, and Materials Conference* (La Jolla, CA), 1993, AIAA, Washington, DC, pp. 628–637 (AIAA Paper 93-1367).

[17]Paz, M., *Structural Dynamics, Theory, and Computation*, 3rd ed., van Nostrand Reinhold, New York, 1991, pp. 437–460.

[18]Heeg, J., Zeiler, T. A., Pototsky, A. S., Spain, C. V., and Engelund, W. C., "Aerothermoelastic Analysis of a NASP Demonstrator Model," *Proceedings of the 34th Structures, Structural Dynamics, and Materials Conference* (La Jolla, CA), 1993, AIAA, Washington, DC, pp. 617–627 (AIAA Paper 93-1366).

[19]Chiang, R. Y., and Safonov, M. G., "Robust Control Toolbox, User's Guide," MathWorks, Inc., Natick, MA, 1992, pp. 1-80–1-86.

[20]Balas, G. J., Doyle, J. C., Glover, K., Packard, A., and Smith, R., "μ-Analysis and Synthesis Toolbox, User's Guide," MathWorks, Inc., Natick, MA, 1991, pp. 1-35–1-47.